J Mater Sci (2010) 45:2732–2746
DOI 10.1007/s10853-010-4261-6

Microcellular processing of polylactide–hyperbranched polyester–nanoclay composites

Srikanth Pilla · Adam Kramschuster · Jungjoo Lee · Craig Clemons · Shaoqin Gong · Lih-Sheng Turng

Received: 20 November 2009 / Accepted: 21 January 2010 / Published online: 4 February 2010

Abstract The effects of addition of hyperbranched polyesters (HBPs) and nanoclay on the material properties of both solid and microcellular polylactide (PLA) produced via a conventional and microcellular injection-molding process, respectively, were investigated. The effects of two different types of HBPs (i.e., Boltorn H2004® and Boltorn H20®) at the same loading level (i.e., 12%), and the same type of HBP at different loading levels (i.e., Boltorn H2004® at 6 and 12%), as well as the simultaneous addition of 12% Boltorn H2004® and 2% Cloisite®30B nanoclay (i.e., HBP–nanoclay) on the thermal and mechanical properties (both static and dynamic), and the cell morphology of the microcellular components were noted. The addition of HBPs and/or HBP with nanoclay decreased the average cell size, and increased the cell density. The stress–strain plots of all the solid and microcellular PLA-H2004 blends showed considerable strain softening and cold drawing, indicating a ductile fracture mode. Among the two HBPs, samples with Boltorn H2004® showed higher strain-at-break and specific toughness compared to Boltorn H20®. Moreover, the sample with Boltorn H2004® and nanoclay exhibited the highest strain-at-break (626% for solid and 406% for microcellular) and specific toughness (405% for solid and 334% for microcellular). Finally, the specific toughness, strain-at-break, and specific strength of microcellular samples were found to be lower than their solid counterparts.

S. Pilla · S. Gong
Department of Mechanical Engineering, University of Wisconsin-Milwaukee, Milwaukee, WI, USA

S. Gong
Department of Materials, University of Wisconsin-Milwaukee, Milwaukee, WI, USA

S. Gong (✉)
Department of Biomedical Engineering, University of Wisconsin, Madison, WI, USA
e-mail: shaoqingong@wisc.edu

A. Kramschuster · J. Lee · L.-S. Turng (✉)
Department of Mechanical Engineering, Polymer Engineering Center, University of Wisconsin, Madison, WI, USA
e-mail: turng@engr.wisc.edu

C. Clemons
Forest Products Laboratory, USDA Forest Service, Madison, WI, USA

Introduction

There is growing interest in developing biobased and biodegradable polymers to help reduce dependency on petroleum-based polymers, reduce the accumulation of persistent plastic waste, and better control the emission of CO_2 in the environment [1–5]. Polylactide (PLA) is popular among biopolymers due to its close proximity in properties to some of the synthetic polymers and its commercial availability at a relatively low cost [6]. In addition to its biobased and biodegradable attributes, PLA is biocompatible; thus, it can be used for biomedical applications such as bone plates, bone screws, tissue repair, and drug delivery [7–15]. In non-biomedical applications, PLA is mainly used in packaging [16]. Despite its many advantages, PLA has a relatively low toughness and a narrow processing window, which limit its widespread applications in areas such as structural components and high-end packaging. For this reason, researchers around the world have been investigating various techniques to improve the toughness and processability of PLA.

The brittleness of PLA can be reduced by copolymerization [17–26], blending with other tough polymers [27–

35], plasticization [36, 37], and by using special additives such as hyperbranched polymers [38–42]. Although copolymerization can be effective in improving the PLA toughness, commercializing a new copolymer is often a long and costly process [43], making them a less viable option when considering large-scale applications of PLA. The major drawback of plasticizers is that during long-term use of the material, they have a tendency to migrate to the surface of the material, causing brittleness [39]. Blending PLA with a tough polymer may improve its toughness effectively, but this generally requires a sufficiently high amount of the tough polymer that can lead to a significant reduction in modulus and strength. Recent studies indicate that hyperbranched polyesters (HBPs) may provide a plausible option to significantly increase the toughness of PLA at a relatively low loading level [38–42]. This is due to the very nature of HBPs, which fall under the category of dendritic polymers and have unique characteristics encompassing highly branched structures with a large number of peripheral functionality [44]. HBPs can be used for a variety of applications such as compatibilizers and toughening agents for plastics, and drug nanocarriers for biomedical applications [45–48]. In this study, HBPs are used as toughers to improve the toughness of PLA while helping to control the cell morphology in the microcellular PLA [38, 39]. Thus far, all the studies on the modification of PLA with HBP have reported the use of conventional injection molding to process the materials [38, 39]. However, in this study, we used the unique microcellular injection-molding process to produce microcellular components based on the PLA–HBP material systems.

The microcellular technology was first reported during 1970s and 1980s by Skripov and co-workers [49] and Suh and co-workers [50]. The microcellular injection molding process takes place in three steps: nucleation, cell growth, and cell stabilization. First, the supercritical fluid (SCF), such as nitrogen or carbon dioxide, acting as the blowing agent, is dissolved into a polymer melt to form a single-phase polymer–gas solution, that is, the polymer melt is super-saturated with the blowing agent. Then, the pressure is suddenly lowered to a value below the saturation pressure triggering a thermodynamic instability and inducing cell nucleation. Cell growth is controlled by the gas diffusion rate and the stiffness of the polymer–gas solution. In general, cell growth is affected by the following factors [51]: (a) time allowed for cells to grow; (b) state of supersaturation; (c) hydrostatic pressure applied to the polymer; (d) temperature of the system; and (e) viscoelastic properties of the single-phase polymer–gas solution. Other than processing parameters, materials formulations such as fillers and polymer blends also have strong influence on cell nucleation and growth. Especially, addition of fillers, which act as nucleating agents, leads to heterogeneous cell nucleation. They provide a large number of nucleation sites leading to higher cell densities and smaller cell sizes [51–59]. A detailed review of the microcellular process is presented in [60].

The employment of SCF such as nitrogen as used in this study reduces the viscosity of the polymer melt [61–63] due to the formation of a single-phase polymer–gas solution, enabling the polymer to be processed at lower temperatures and pressures [64, 65]. This is a very desirable feature for biobased polymers such as PLA, which are moisture and heat sensitive. Microcellular plastics are characterized by cell densities on the order of 10^7–10^9 cells/cm^3 and cell sizes on the order of several tens of microns or less. Compared to microcellular plastics, conventional foamed plastics possess relatively lower cell densities (in the range of 10^3–10^6 cells/cm^3) and larger cell size (on the order of 100 μm or more), thus leading to inferior material properties [66]. Compared with the conventional injection molding process, the microcellular injection-molding process produces components with increased dimensional stability, less thermal degradation, and less material [52–54].

This study investigated PLA–HBP blends produced via microcellular injection molding using two types of HBP polymers. Poly (maleic anhydride-*alt*-1-octadecene) was used as a cross-linking agent for the HBP. Specimens have also been produced using conventional injection molding to compare with foamed specimens. Finally 2% nanoclay was used to study the effect of nanofillers on the properties of PLA–HBP blends. More information on PLA–nanoclay nanocomposites can be found in [52, 67, 68].

Experimental

Materials

Polylactide (NatureWorks™ PLA 3001D) in pellet form was obtained from NatureWorks® LLC (Minnetonka, MN). It has a specific gravity of 1.24 and a melt flow index around 15 g/10 min. PLA 3001D was synthesized from approximately 92% L-lactide and 8% meso-lactide [69]. The HBPs, under the trade names Boltorn H20® and Boltorn H2004® were provided by Perstorp Speciality Chemicals AB, Sweden. Boltorn H20® has a nominal molecular weight of 1750 g/mol and consists of 16 primary hydroxyl (OH–) groups; Boltorn H2004® has a nominal molecular weight of 3100 g/mol and possesses six hydroxyl (OH–) groups. Poly (maleic anhydride-*alt*-1-octadecene) (PA) obtained from Sigma–Aldrich®, was used as a cross-linking agent for the HBPs. It has a number average molecular weight of 30,000–50,000 g/mol and is a copolymer of octadecene and maleic anhydride. The organically modified montmorillonite

(MMT) nanoclay, Cloisite®30B, was supplied by Southern Clay Products, Inc. The nanoclay was surface treated by an ion exchange reaction between Na^+ existing in the gallery of the nanoclay and quaternary ammonium cations. Cloisite®30B was modified with bis-(2-hydroxyethyl) methyl (hydrogenated tallowalkyl) ammonium cations.

Methods

Processing

The PLA was combined with PA, HBP (Boltorn H20® and Boltorn H2004®), and nanoclay (Cloisite®30B) (used as received) into a variety of formulations, with Naugard-10 and Naugard-524 introduced as antioxidants. Table 1 presents the formulations compounded, injection–molded, and evaluated in this study. PA was used in the formulations because previous study has indicated that greater toughening effect can be achieved due to the formation of a network between HBP and PA resulting from a reaction between the HBPs' hydroxyl groups and the PA's anhydride groups during the melt compounding process [38]. Also among the HBPs, Boltorn H20® has 16 hydroxyl (–OH) functional groups and Boltorn H2004® has six hydroxyl (–OH) functional groups. Therefore, based on their reactivity with polyanhydride (PA), required amounts of HBPs have been computed. Therefore, though the overall percentage of the HBP + PA remains the same, the constituent weights vary due to the different amount of reactive groups on the periphery of individual HBPs.

Prior to compounding and injection-molding, several master batches were created using a thermokinetic mixer (k-mixer). All the master batches were compounded in quantities of 200 g. The rotor speed was 4000 rpm, and the discharge temperature was either 175 °C (for master batches containing PLA with PA, the antioxidants, and the nanoclay, if used) or 80 °C (for a master batch consisting of Boltorn H20® and PA for Experiment #5). After discharging, the molten blend was pressed into a flat sheet, and subsequently granulated. The contents of the master batches created are provided in Table 2. For Experiments 1 and 5 (Table 2), master batches of PLA, Naugard-10, and Naugard-524 were created. For Experiments #2 and 3, master batches of PLA, PA, Naugard-10, and Naugard-524 were created, while for Experiment #4, Cloisite®30B nanoclays were added. Boltorn H2004® comes in a liquid form and was added to these formulations during twin-screw compounding using a Cole-Parmer peristaltic pump (model #7553–80).

All of these master batches were then let-down with PLA at the appropriate ratio to achieve the formulations described in Table 1. The co-rotating, twin-screw compounding extruder had a screw diameter of 32 mm and an L/D ratio of 36.25. The materials were all fed into the main feed throat and extruded at 11.4 kg/h (the pumping rate of the peristaltic pump was set at 8.5 g/min for Experiment #2, and 17 g/min for Experiments #3 and #4) with a screw speed of 200 rpms and a melt temperature of approximately 170–180 °C to create the formulations described in Table 1.

Tensile bars (ASTM D638-03, Type I) were injection-molded using an Arburg Allrounder 320S (Lossburg, Germany) with a 25-mm diameter screw and equipped with microcellular (under the trade name MuCell®) technology (Trexel, Inc., Woburn, MA). Solid and microcellular tensile bars were molded at the processing conditions

Table 1 Percent composition of the materials compounded

Experiment	Sample	PLA	PA	HBP	Naugard-10 (0.2 wt% total formulation)	Naugard-524 (0.2 wt% total formulation)	Cloisite®30B
1	PLA	99.6	0.0	0	0.2	0.2	0
2	PLA–6%(H2004 + PA)	93.6	1.5	4.5	0.2	0.2	0
3	PLA–12%(H2004 + PA)	87.6	3.0	9.0	0.2	0.2	0
4	PLA–12%(H2004 + PA)–2%NC	85.6	3.0	9.0	0.2	0.2	2
5	PLA–12%(H20 + PA)	87.6	7.4	4.6	0.2	0.2	0

Table 2 Master batches created for compounding

Master batch	PLA	PA	HBP	Naugard-10	Naugard-524	Cloisite®30B
Exps 1, 5	X			X	X	
Exps 2, 3	X	X	Added during twin screw extrusion	X	X	
Exp 4	X	X	Added during twin screw extrusion	X	X	X

Table 3 Injection-molding conditions used to mold the tensile bars (*S* solid, *M* microcellular)

	S	M
Mold temperature (°C)	20	20
Nozzle temperature (°C)	175	170
Injection speed (cm^3/s)	20	20
wt% SCF content	n/a	0.56
Pack pressure (bar)	795	–
Pack time (s)	7.5	–
Screw recovery speed (RPM)	280	280
Cooling time (s)	35	35
Microcellular process pressure (bar)	n/a	190

indicated in Table 3. The processing temperatures for both the extrusion and injection molding processes were kept between 170 and 180 °C to avoid significant PLA thermal degradation. Note that with conventional injection-molding, supercritical nitrogen fluid (SCF) was not introduced into the material. In addition, the pack/hold stage is absent in microcellular injection molding due to the homogeneous packing pressure that results from the nucleation and growth of cells [65], which was shown to drastically reduce the shrinkage and warpage of microcellular injection-molded parts when compared with conventional injection molding, thereby greatly enhancing the dimensional stability of molded parts with a complex geometry [55]. A slight variation in the wt% SCF content is observed for the microcellular injection-molded samples. This can be attributed to varying shot weights between the neat resin and the composites. This shot weight is used to compute the wt% SCF, shown in Eq. 1 [53]

$$\text{wt\%SCF} = \frac{\dot{m}t(27.8)}{m} \tag{1}$$

where $\dot{m}$ is the mass flow rate of the SCF (kg/h), t is the SCF dosage time (s), m is the shot weight (g), and 27.8 is a conversion factor.

Wide-angle X-ray diffraction

WAXRD analysis was performed on Scintag XDS 2000 with Ni-filtered Cu Kα radiation (1.5418 A°) at room temperature in the range of $2\theta = 1.5$–9° with a scanning rate of 1°/min.

Differential scanning calorimetry (DSC)

A differential scanning calorimeter (TA Instruments, DSC-Q20) was used to study the thermal properties of the blend materials. From each sample, 8–10 mg was sliced from the injection-molded specimens and placed in a hermetically sealed aluminum pan under 50 mL/min nitrogen flow. The samples were first heated from 40 °C to 180 °C and then subjected to an isothermal stage for 3 min, cooled to 0 °C, and finally reheated to 200 °C. The ramp speed in all of the heating and cooling processes was 10 °C/min.

The degree of crystallinity of PLA was computed using Eq. 2 [70]:

$$\chi_c(\%\,\text{Crystallinity}) = \frac{\Delta H_m}{\Delta H_m^0} \times \frac{100}{w} \tag{2}$$

where ΔH_m is the enthalpy for melting, ΔH_m^0 is the enthalpy of melting for a 100% crystalline PLA sample, which is 93.7 J/g, and w is the weight fraction of PLA in the sample.

In order to determine the degree of crystallinity of the sample, the extra heat absorbed by the crystallites formed during heating (i.e., cold crystallization) had to be subtracted from the total endothermic heat flow due to the melting of the total amount of crystallites [71]. Thus, the modified equation can be written as follows:

$$\chi_c(\%\,\text{Crystallinity}) = \frac{\Delta H_m - \Delta H_{cc}}{\Delta H_m^0} \times \frac{100}{w} \tag{3}$$

where ΔH_{cc} is the cold crystallization enthalpy.

Scanning electron microscopy (SEM)

The fracture surfaces obtained from the tensile tests were examined using SEM (Hitachi S-570) operated at 10 kV. All the specimens were sputter coated with a thin layer of gold ($\sim$20 nm) prior to examination.

Transmission electron microscopy (TEM)

The structure of the PLA–HBP blends were investigated using a Hitachi H-600 TEM operated at 75 kV. The ultra-thin sections with a thickness of $\sim$70 nm were microtomed at room temperature ($\sim$25 °C) using an RMC ultramicrotome (Model# MT-7000). No stain was used. The TEM sections were taken from the middle portion of the tensile test specimens.

Dynamic mechanical analysis (DMA)

The dynamic mechanical analysis measurements were performed on a TA Q800 DMA instrument in single cantilever mode. The dimensions of the rectangular samples were about 17.6 × 12.7 × 3.2 mm^3. Samples were heated at a rate of 3 °C/min ranging from 0 °C to 85 °C with a frequency of 1 Hz and a strain of 0.02%, which is in the linear viscoelastic region, as determined by a strain sweep.

Tensile testing

The static tensile properties (i.e., modulus, strength, strain-at-break, and toughness) were measured at room temperature (~25 °C) and atmospheric conditions (relative humidity of ~50 ± 5%) with a 50-kN load cell on an Instron Model 3369 tensile tester. The crosshead speed was set at 5 mm/min. All the tests were carried out according to the ASTM standard (ASTM-D638); five specimens of each sample were tested and the average results were reported.

Results and discussions

WAXRD analysis

The structure of the solid and microcellular PLA–12%(H2004 + PA)–2%Nanoclay composite was studied using wide angle X-ray diffraction (WAXRD). The WAXRD pattern provides a convenient way to determine the degree of clay dispersion based on the diffraction angle (2θ), shape, and intensity of the (001) diffraction peak from the nanoclays dispersed in the polymer matrix. In general, when the nanoclay are fully exfoliated the X-ray diffraction peaks disappear, but if the nanoclay is intercalated then the diffraction peak shifts to lower angles due to the increase in the interlayer gallery spacing (d_{001}).

Figure 1 shows the WAXRD pattern of nanoclay and PLA–12%(H2004 + PA)–2%Nanoclay composites (both solid and microcellular). For reference, the WAXRD patterns of solid and microcellular PLA–12%(H2004 + PA) without nanoclay are also presented. As shown in the figure, the diffraction peaks from the nanoclays in both the solid and microcellular PLA–12%(H2004 + PA)–2%Nanoclay composites shifted to lower angles. The diffraction peak

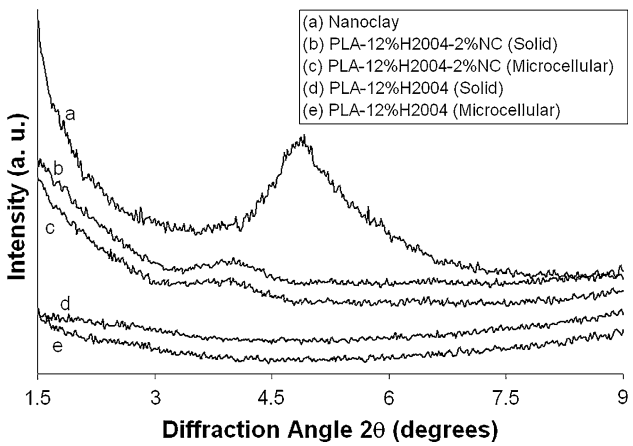

Fig. 1 WAXRD patterns of Nanoclay (30B), solid and microcellular PLA–12%(H2004 + PA) and PLA–12%(H2004 + PA)–2%Nanoclay composites

angle (2θ) for the (001) peak of the as-received nanoclay (Cloisite®30B) was 4.74°. For this diffraction angle, the basal spacing for the nanoclay, as per the Bragg's diffraction equation, is $d_{001} = 1.86$ nm. This compares reasonably well with the information provided by the manufacturer. For both the solid and microcellular PLA–12%(H2004 + PA)–2%Nanoclay composites, the diffraction peaks were observed at $2\theta = 3.9°$, and the corresponding basal spacing was calculated to be $d_{001} = 2.3$ nm. As stated above, an increase in the interlayer basal spacing is indicative of an intercalated structure. Thus, as noted in the previous studies, the PLA molecules intercalated into the clay layers during the melt compounding process and increased the interlayer spacing [54], but the clay was not exfoliated. A visual examination of this inference was made using TEM, as discussed in the next section.

Morphological properties

Microstructure analysis via TEM

Figure 2a, b shows the TEM images of the solid and microcellular PLA–12%(H2004 + PA)–2%Nanoclay composites, respectively. The dark lines are the clay particles and bright area is the PLA matrix. The degree of nanoclay dispersion was similar in the solid and microcellular specimens. The degree of nanoclay dispersion generally depends on the interaction between the nanoclays and the polymer matrix. The TEM images clearly showed that nanoclays were dispersed quite uniformly in the polymer matrix, mostly showing an intercalated structure occasionally with a few larger nanoclay agglomerates observed here and there. The inset in Fig. 2c shows an enlarged view of the microcellular PLA–12%(H2004 + PA)–2%Nanoclay composite with an intercalated structure. These results agree with the XRD results shown in Fig. 1.

Figure 3 shows the TEM images of the solid and microcellular PLA–HBP blends. The dark particles (shown by black arrows) and the dark lines are (HBP + PA) and the bright area is the PLA matrix. The tiny microcells in the microcellular samples are indicated by white arrows. Figure 3a, b shows the TEM images of the solid and microcellular PLA–6%(H2004 + PA), respectively, in which the average size of the individual (H2004 + PA) particles ranged from approximately 10–100 nm. Figure 3c, d shows the TEM images of solid and microcellular PLA–12%(H2004 + PA), respectively. Compared with PLA–6%(H2004 + PA), a much more homogeneous (H2004 + PA) distribution was achieved in the PLA–12%(H2004 + PA) sample. Figure 3e, f shows, respectively, the TEM images of solid and microcellular PLA–12%(H2004 + PA)–2%Nanoclay composites. In this case, the dark regions indicate both the (HBP + PA) and nanoclays.

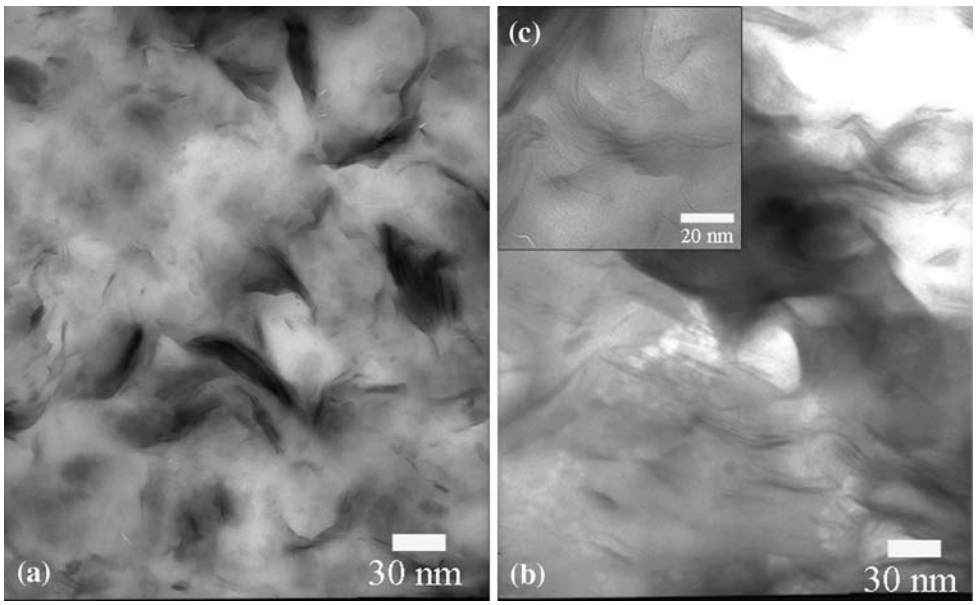

Fig. 2 TEM images of PLA–12%(H2004 + PA)–2%Nanoclay composite: **a** PLA–12%(H2004 + PA)–2%Nanoclay (Solid), **b** PLA–12%(H2004 + PA)–2%Nanoclay (Microcellular), **c** enlarged view of the PLA–12%(H2004 + PA)–2%Nanoclay (Microcellular)

Finally, the TEM images of PLA–12%(H20 + PA) are shown in Fig. 3g, h. Similar to the PLA–12%(H2004 + PA) sample, both dark particles and dark lines are shown in the TEM images of PLA–12%(H20 + PA); however, the overall dispersion of the 12%(H20 + PA) in the PLA was less homogenous than that of the 12%(H2004 + PA) in the PLA.

Fracture surface analysis via SEM

Figure 4 shows representative SEM images of the solid (images on the left) and microcellular (images on the right) PLA and PLA–HBP blends. All images were taken at the same magnification of ×100 (scale bar: 100 μm). The SEM images provide information on the microstructure, including the cell morphology in microcellular specimens and the fracture behaviors of the specimens [52–57, 64, 65, 72].

The fracture surface of the solid PLA (Fig. 4a) was smooth without obvious plastic deformation indicating brittle behavior. For the solid PLA–HBP blends, the fracture surfaces (Fig. 4c, e, g, i) were much rougher, indicating plastic deformation. In general, the microcellular specimens showed similar morphological deformation as that of the solid samples.

The average cell size and cell density were quantitatively determined using an image analysis tool (UTHSCSA ImageTool).

The cell density was calculated using [73]:

$$\text{Cell density} = \left(\frac{N}{L^2}\right)^{3/2} M \tag{4}$$

where N is the number of cells, L is the linear length of the area, and M is a unit conversion factor resulting in the number of cells per cm^3.

The graphical results of the average cell size and cell density of the microcellular samples are shown in Fig. 5. The left set of plots show the effect of (H2004 + PA) on cell size and density with variation in the (H2004 + PA) content and composition (with or without nanoclay) and the right set of plots shows the effects of addition of different types of HBPs (H20 vs. H2004) on cell size and density. The average cell size of pure PLA was 39 μm. With the addition of 6%(H2004 + PA), the average cell size decreased to 31 μm. Increasing the content of (H2004 + PA) to 12%, that is for the PLA–12%(H2004 + PA) sample, the average cell size decreased to 16 μm and with the addition of 2% nanoclay, that is, for the PLA–12%(H2004 + PA)–2%Nanoclay composite, the average cell size reduced to 10 μm. However, with the addition of 12%(H20 + PA), that is for the PLA–12%(H20 + PA), the average cell size decreased to 31 μm, which was higher than 16 μm achieved for PLA–12%(H2004 + PA).

The cell density increased by about 1.2 and 5 times for the PLA–6%(H2004 + PA) and PLA–12%(H2004 + PA) samples compared with pure PLA. Furthermore, with the addition of 2% nanoclay, that is for the PLA–12%(H2004 + PA)–2%Nanoclay composite, the cell density increased 10 times compared with that of the microcellular pure PLA; however, for the PLA–12%(H20 + PA), the cell density increased by approximately 1.1 times. Thus, compared with the microcellular PLA–12%(H2004 + PA) specimen, microcellular PLA–12%(H20 + PA) showed

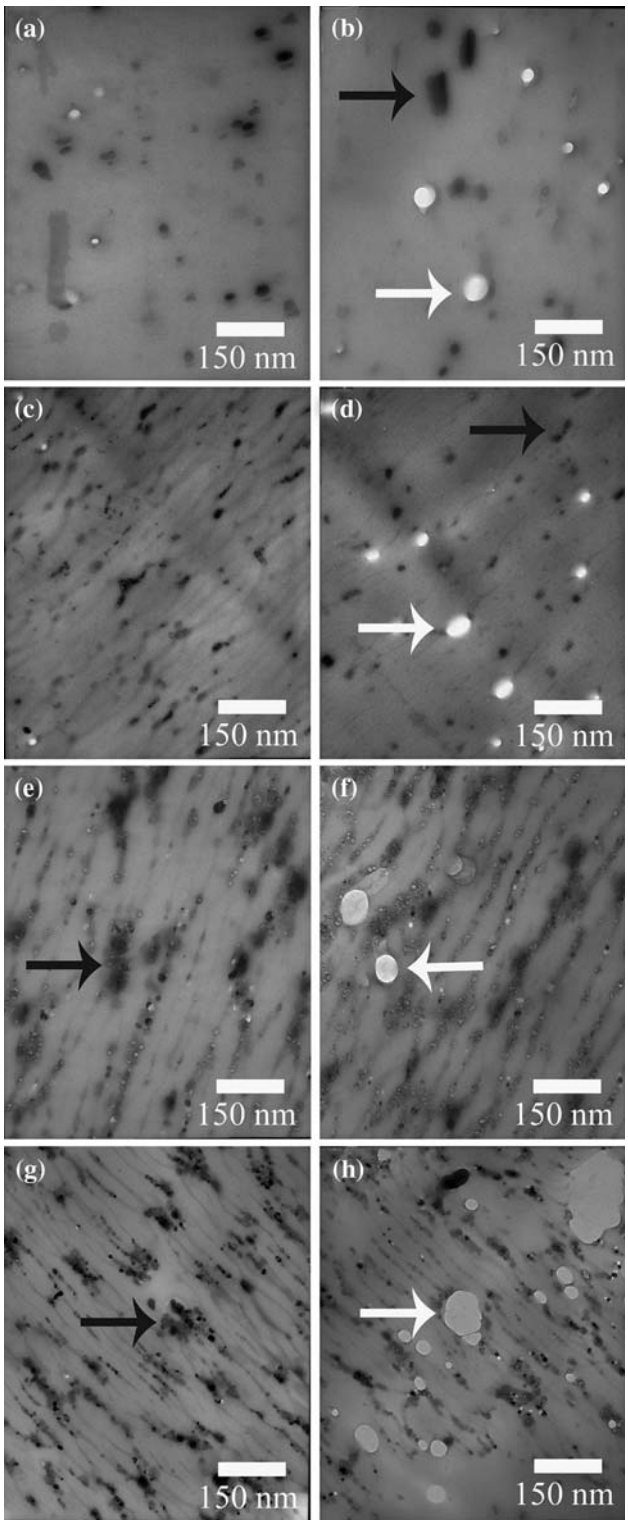

Fig. 3 TEM images of solid and microcellular PLA–HBP blends: **a** PLA–6%(H2004 + PA) (Solid), **b** PLA–6%(H2004 + PA) (Microcellular), **c** PLA–12%(H2004 + PA) (Solid), **d** PLA–12% (H2004 + PA) (Microcellular), **e** PLA–12%(H2004 + PA)–2% Nanoclay (Solid), **f** PLA–12%(H2004 + PA)–2%Nanoclay (Microcellular), **g** PLA–12%(H20 + PA) (Solid), **h** PLA–12%(H20 + PA) (Microcellular)

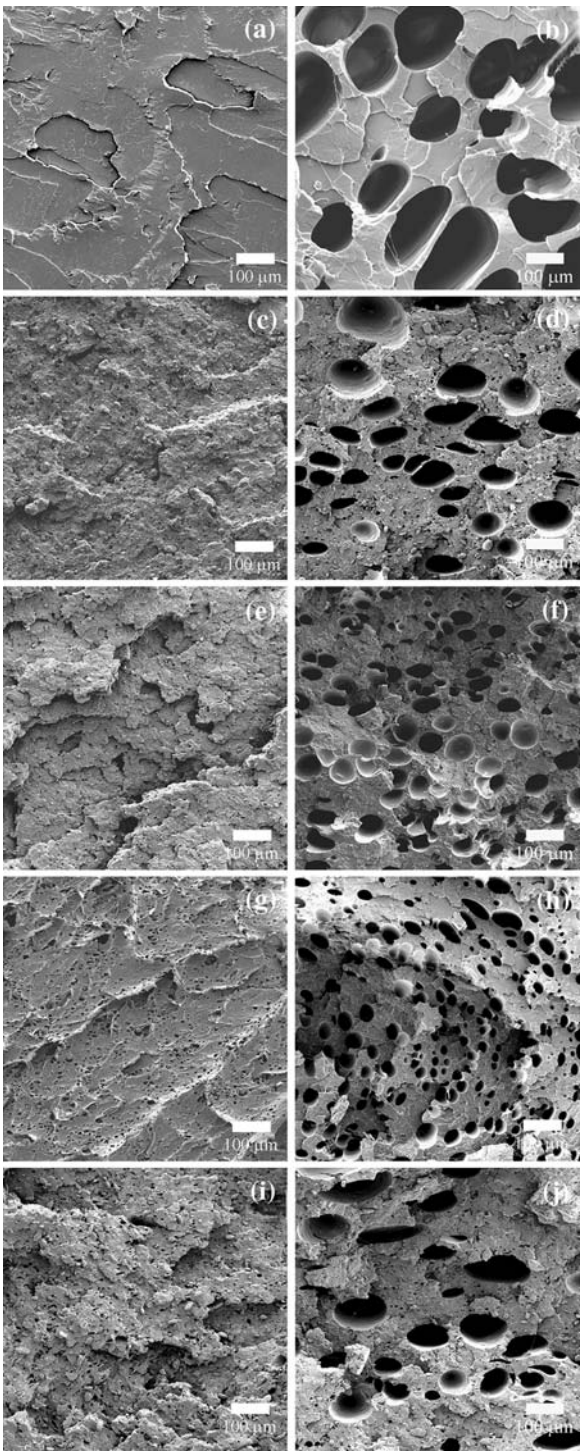

Fig. 4 Representative SEM images of the fracture surfaces of solid and microcellular PLA and PLA–HBP blends: **a** pure PLA (Solid), **b** pure PLA (Microcellular), **c** PLA–6%(H2004 + PA) (Solid), **d** PLA–6% (H2004 + PA) (Microcellular), **e** PLA–12%(H2004 + PA) (Solid), **f** PLA–12%(H2004 + PA) (Microcellular), **g** PLA–12%(H2004 + PA)–2%Nanoclay (Solid), **h** PLA–12%(H2004 + PA)–2%Nanoclay (Microcellular), **i** PLA–12%(H20 + PA) (Solid), **j** PLA–12%(H20 + PA) (Microcellular)

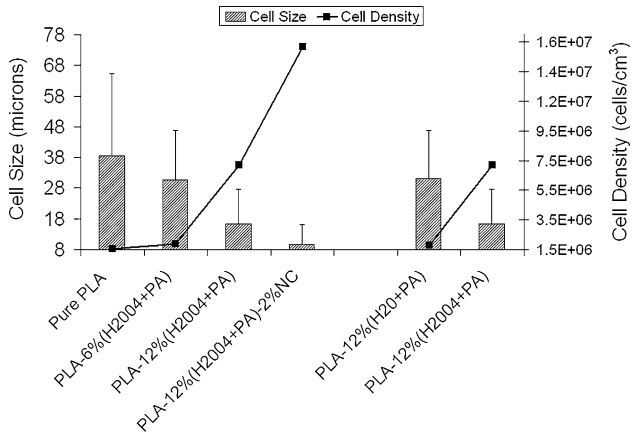

Fig. 5 The average cell size and cell density of microcellular PLA and PLA–HBP blends

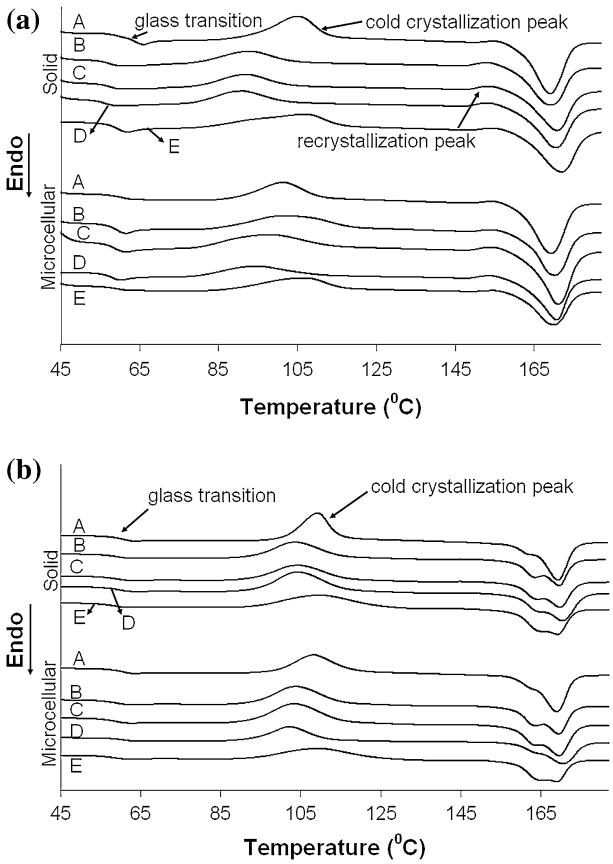

Fig. 6 Melting curves of solid and microcellular PLA and PLA–HBP blends. Data obtained from **a** first heating run and **b** second heating run; (*a*) pure PLA, (*b*) PLA–6%(H2004 + PA), (*c*) PLA–12%(H2004 + PA), (*d*) PLA–12%(H2004 + PA)–2%Nanoclay, (*e*) PLA–12%(H20 + PA)

inferior cell structure (larger cell size and lower cell density). Therefore, it is evident that the effect of H20 + PA on the cell structure of PLA was meager. On the other hand, it can be inferred that the H2004 + PA had a positive effect on the cellular morphology of PLA. Moreover, addition of nanoclay increased the cell density almost 10 times and decreased the cell size by 75%. This increase in cell density and decrease in cell size can be attributed to: (1) more cells being nucleated in the presence of nanoclay resulting in less SCF available for each cell to grow, thereby reducing cell size; or (2) increase in melt viscosity due to the addition of nanoclay thereby inducing strain hardening and thus hindering cell growth and coalescence, and reducing cell size [74]. These results agree with the findings from the literature that addition of fillers decreases cell size and increases cell density [58, 59, 65, 75]. Thus, nanoclay acted as a nucleating agent, thereby promoting heterogeneous cell nucleation and led to more uniform cell nucleation and growth behavior.

Finally, it should be noted that cell size and distribution are not always uniform due to the dynamic nature of the microcellular injection-molding process. The quantitative analyses presented in Fig. 5 include representative values taken from the center portion of the cross section of the tensile bars. However, cell size and cell density varies throughout the thickness of the part due to shear and rapid cooling at the polymer–mold interface, as well as other phenomena. More specifically, there is a typical solid skin layer near the polymer–mold interface where cells are not visible due to rapid cooling of the material, which hampered cell growth.

Thermal properties

The thermal properties of PLA and PLA–HBP blends, including crystallization and melting behavior, were investigated using DSC. The thermograms and the numerical values of temperature and enthalpy obtained from the first and second heating cycles are shown in Fig. 6 and Table 4, respectively. The data obtained from the first heating cycle provide the thermal history of the injection-molded samples, while the data obtained from the second heating cycle allows for a direct comparison of the crystallization behavior of different materials after erasing the thermal history through the first heating cycle.

First heating cycle

As shown in Fig. 6a, an endothermic peak exists near the glass transition phase of solid PLA, solid PLA–12%(H20 + PA), microcellular PLA–6%(H2004 + PA), microcellular PLA–12%(H2004 + PA) and microcellular PLA–12%(H2004 + PA)–2%Nanoclay composite. This is due to physical aging of the polymeric materials [76–78] and is related to the inherent distribution of the relaxation times of polymer chains [79]. Also, two crystallization peaks were observed for all the solid and microcellular

Table 4 Thermal characteristics of PLA and PLA–HBP blends

Sample #	Cold crystallization		Recrystallization		Melting			Degree of crystallinity
	Temp (°C)	Enthalpy (J/g)	Temp (°C)	Enthalpy (J/g)	Temp (°C)		Enthalpy J/g	χ (%)
Solid (first heating)								
PLA	105.2	−27.6	155.5	−0.7	169.1		34.9	8
PLA–6%(H2004 + PA)	92.1	−24.8	153.6	−1.9	169.2		36.7	11
PLA–12%(H2004 + PA)	91.4	−22.6	154.2	−2.1	170.8		36.4	14
PLA–12%(H2004 + PA)–2%NC	90.6	−20.3	153.5	−1.4	170.5		35.8	18
PLA–12%(H20 + PA)	107.2	−23.3	154.9	−0.7	171.9		34.6	13
PLA–12%(H2004 + PA)	91.4	−22.6	154.2	−2.1	170.8		36.4	14
Microcellular (first heating)								
PLA	101.9	−24.6	155.4	−1.7	169.4		35.1	9
PLA–6%(H2004 + PA)	101.1	−24.7	155.0	−1.1	170.2		35.7	11
PLA–12%(H2004 + PA)	98.3	−24.4	154.8	−1.7	171.1		37.1	13
PLA–12%(H2004 + PA)–2%NC	94.7	−19.8	154.2	−1.5	170.7		36.1	18
PLA–12%(H20 + PA)	105.2	−22.2	154.7	−0.4	169.9		33.7	13
PLA–12%(H2004 + PA)	98.3	−24.4	154.8	−1.7	171.1		37.1	13
Solid (second heating)								
PLA	109.1	−26.8	–	–	162.8	169.3	36.4	10
PLA–6%(H2004 + PA)	104.5	−28.7	–	–	163.9	169.6	39.1	12
PLA–12%(H2004 + PA)	104.3	−27.1	–	–	164.6	169.8	38.4	14
PLA–12%(H2004 + PA)–2%NC	103.9	−25.2	–	–	165.1	170.4	38.7	17
PLA–12%(H20 + PA)	111.2	−27.2	–	–	165.4	169.2	37.6	13
PLA–12%(H2004 + PA)	104.3	−27.1	–	–	164.6	169.8	38.4	14
Microcellular (second heating)								
PLA	108.1	−26.6	–	–	163.2	169.1	36.9	11
PLA–6%(H2004 + PA)	104.3	−28.2	–	–	164.1	169.5	38.5	12
PLA–12%(H2004 + PA)	103.6	−26.8	–	–	164.2	169.6	38.8	15
PLA–12%(H2004 + PA)–2%NC	102.4	−22.2	–	–	164.3	170.4	35.6	17
PLA–12%(H20 + PA)	110.7	−27.1	–	–	165.1	169.1	37.4	13
PLA–12%(H2004 + PA)	103.6	−26.8	–	–	164.2	169.6	38.8	15

specimens. The first peak is referred to as *cold-crystallization peak* and the second peak as *recrystallization peak*. With the addition of (H2004 + PA) (6% or 12%), the peak temperatures of the cold-crystallization peaks decreased. This indicates that the addition of (H2004 + PA) promoted initial cold crystallization of the PLA material. Moreover, with the addition of 2% nanoclay, a similar decreasing trend in the cold-crystallization peak temperature was observed. On the contrary, the addition of 12%(H20 + PA) increased the cold-crystallization peak temperature, indicating that the crystallization process was partially delayed during the heating cycle. The recrystallization peaks, which occurred due to the restructuring of certain existing crystalline structures at higher temperatures [5], appeared just before the melting peaks for all the solid and microcellular specimens.

Table 4 shows the numerical values of temperatures and enthalpies from the first heating curve of the PLA and PLA–HBP blends. The enthalpies of the cold-crystallization peaks decreased with the addition of 6% and 12%(H2004 + PA) HBPs, indicating that there was enhanced PLA crystallization during the cooling during injection molding. As a result, there was a higher crystallinity and a less cold crystallization. Moreover, with the addition of 2% nanoclay, the enthalpy of cold crystallization also decreased, indicating further enhancement of crystallization during cooling. Indeed, as shown in Table 4, the degree of crystallinity (computed using Eq. 3) of all the PLA–HBP blends was observed to be higher than that of the pure PLA. This agrees with the findings reported in the literature that addition of HBP enhanced the degree of crystallinity in PLA [39, 42]. Furthermore, nanoclay acted

as crystallization nucleating agents and further increased degree of crystallinity [52, 53, 56, 80, 81]. Although the cold crystallization peak temperature was higher in the PLA–12%(H20 + PA) specimen, the degree of crystallinity in this sample was similar to the PLA–12%(H2004 + PA) specimen. Among all the solid and microcellular samples, the degree of crystallinity was observed to be the highest (18% for both solid and microcellular) for PLA–12%(H2004 + PA–2%Nanoclay composite. Finally, no significant difference was observed between the degree of crystallinity of the corresponding solid and microcellular samples.

Second heating cycle

Figure 6b and Table 4 show the thermogram and numerically analyzed data of PLA and PLA–HBP blends, respectively, from the second heating cycle. Unlike in the first heating cycle, no endotherm peaks were observed near the glass transition temperature (T_g) because the enthalpic recovery that occurred during the first heating cycle is kinetic in nature [5]. Also, only one crystallization peak, that is, cold-crystallization was observed. Similar to the first heating cycle, the addition of (H2004 + PA) (6% or 12%) decreased the peak temperatures of the cold-crystallization peaks. This indicates that the addition of H2004 promoted the cold crystallization of the PLA material. Again, as previously observed, for the PLA–12%(H2004 + PA)–2%Nanoclay composite, the cold-crystallization peak temperature did not change. Also, as in the case of the first heating cycle, the addition of 12%(H20 + PA) increased the cold-crystallization peak temperature of PLA by a few degrees. The degree of crystallinity of all the samples was found to be either the same or slightly higher than that obtained during the first heating cycle.

Double melting peaks were obtained for all the specimens during the second heating cycles (Fig. 6b; Table 4). This is commonly observed [82] and, in our case, may be due to the differences in crystalline morphology (e.g., lamellar thickness or spherulite size) from melt and cold crystallization, for instance, which may have slightly different melt temperatures [83].

Weight reduction of the microcellular samples

The weight of PLA without HBP and PA was reduced by 16% using microcellular injection molding. Addition of 12%(H20 + PA) yielded blends with the least weight reduction (10%). Though the weight was only reduced by 11% in blends with 6%(H2004 + PA), doubling the additive content yielded similar weight reductions (15%) as with the pure PLA (16%). When 2% nanoclay was added to the PLA–12%(H2004 + PA) blend, the weight reduction dropped to 13%.

Overall, the variation in weight reduction among all the samples was due to the effects of the blend composition on the behavior of cell nucleation and growth, different pressure-specific volume–temperature (pvT) properties that affect the melt properties of these materials and the processing parameters such as SCF dosage time, and the dynamic nature of the microcellular injection molding.

Dynamic mechanical properties (DMA)

The viscoelastic properties of PLA and the PLA–HBP blends were studied using DMA. The DMA properties reported here are the actual properties measured for the solid and microcellular specimens without taking into account the weight reduction of the microcellular specimens. In general, a declining trend was observed for the storage moduli of all the solid and microcellular specimens with respect to temperature with the most rapid reduction occurring at the glass transition region (Fig. 7). In the glassy region (<55 °C), the storage modulus of the solid specimen

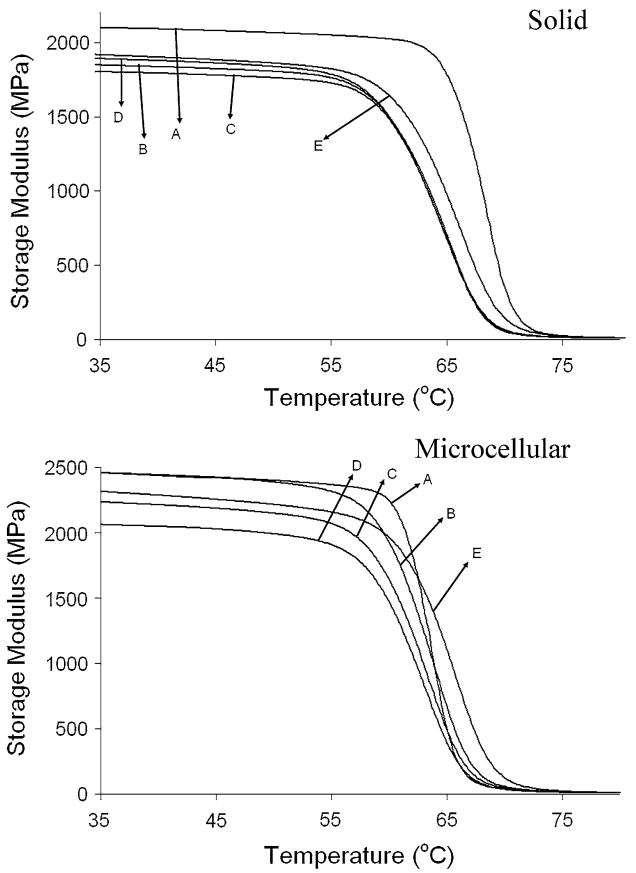

Fig. 7 Storage moduli of solid and microcellular PLA and PLA–HBP blends: (*a*) pure PLA, (*b*) PLA–6%(H2004 + PA), (*c*) PLA–12%(H2004 + PA), (*d*) PLA–12%(H2004 + PA)–2%Nanoclay, (*e*) PLA–12%(H20 + PA)

decreased with increasing (H2004 + PA). Addition of 2% nanoclay increased the storage modulus of the solid specimen (i.e., PLA–12%(H2004 + PA)–2%Nanoclay composite), but it was still lower than that of the solid PLA. Similarly, addition of 12%(H20 + PA) decreased the storage modulus of the solid specimen. Furthermore, addition of H2004 reduced storage modulus more than that due to the addition of H20 at the same 12% loading level. This is probably due to the larger number of –OH groups (16) on the periphery of H20 compared with H2004 (6), resulting in a higher cross-link density after reacting with PA. In the glass transition region, no cross-over was observed in any solid samples, and the same trend of storage modulus as seen in the glassy region continued. Above the glass transition region (temperatures above 70 °C), no significant difference was observed in the storage moduli of all the solid specimens.

For the microcellular specimens (Fig. 7), in general, the storage modulus followed a similar trend as that of the solid samples, except that in the glassy region, the difference between the storage modulus of microcellular PLA and microcellular PLA–6%(H2004 + PA) was very minimal. Also, the storage modulus of microcellular PLA–12%(H2004 + PA)–2%Nanoclay composite was found to be lower than that of microcellular PLA–12%(H2004 + PA). In the glass transition region, a cross-over was observed between the microcellular PLA and microcellular PLA–6%(H2004 + PA). The slightly different trend observed in the solid and microcellular samples may be attributed to the variation of weight reduction and cell morphology in these microcellular specimens. Above the glass transition region, no significant difference was observed in the storage moduli of all the microcellular specimens. Finally, the storage moduli of the microcellular samples was found to be higher than their solid counterparts due to the introduction of microcells [52].

The glass transition temperatures (T_g) obtained from the peaks of the Tan-δ curves are tabulated in Table 5. The T_g of all solid PLA–HBP blends were lower than that of the solid PLA. This is consistent with previously published results [38, 40]. However, the T_g of the microcellular PLA–HBP blends was higher than that of the microcellular PLA. Also, the T_g of the microcellular specimens were found to be lower than their solid counterparts, which agrees with our previous results [52, 53, 57]. This might be due to the increased molecular mobility due to the presence of microcells in the microcellular specimens.

Figure 8 shows the area under the tan-δ curves of all the solid and microcellular samples. In general, a larger area underneath the tan-δ peak indicates that the molecular chains exhibit a higher degree of mobility and, therefore, have increased damping capability [84]. As shown in Table 5, the

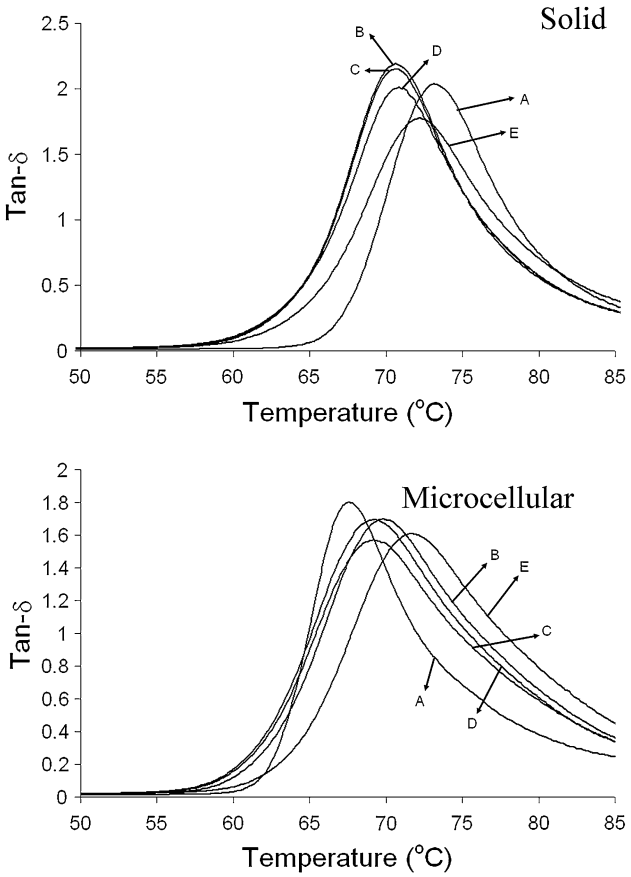

Fig. 8 Tan-δ curves of solid and microcellular PLA and PLA–HBP blends: (*a*) pure PLA, (*b*) PLA–6%(H2004 + PA), (*c*) PLA–12%(H2004 + PA), (*d*) PLA–12%(H2004 + PA)–2%Nanoclay, (*e*) PLA–12%(H20 + PA)

Table 5 The glass transition temperatures and area integration under the tan-δ curves of solid and microcellular PLA and PLA–HBP blends measured using DMA

Samples	T_g (°C)		Area under the tan-δ curve (cm^2)	
	Solid	Microcellular	Solid	Microcellular
PLA	73.2	67.5	73.2	67.5
PLA–6%(H2004 + PA)	70.7	69.9	70.7	69.9
PLA–12%(H2004 + PA)	70.3	69.3	70.3	69.3
PLA–12%(H2004 + PA)–2%NC	70.9	69.1	70.9	69.1
PLA–12%(H20 + PA)	72.1	71.8	72.1	71.8

area under the tan-δ curve increased with the addition of 6% or 12% (H2004 + PA). Thus, the damping ability, that is, the energy absorption capacity of PLA, improved with addition of (H2004 + PA). Also, the area under the tan-δ curve was similar between PLA–12%(H2004 + PA) and PLA–12%(H2004 + PA)–2%Nanoclay. On the other hand, the addition of (H20 + PA) did not change the area under the Tan-δ curve of PLA. This shows that (H20 + PA) did not effectively toughen the PLA matrix.

Static mechanical properties

Figures 9 and 10 show the stress–strain plots and specific mechanical properties of the PLA and the PLA–HBP blends, respectively, obtained by tensile testing of the solid and microcellular specimens. The specific properties such as specific toughness, specific strength, and specific modulus were obtained by dividing the static properties with the density of the respective material.

Considerable necking was observed for all the solid and microcellular samples (Fig. 9). Solid PLA underwent strain softening but addition of 6%(H2004 + PA) induced considerable cold drawing and ductile failure. A similar trend of strain softening and cold drawing was observed when the (H2004 + PA) content was increased to 12%, except that the cold drawing was greater than in the solid PLA–6%(H2004 + PA). Further, for the solid PLA–12%(H2004 + PA)–2%Nanoclay composite, the cold drawing was the greatest among all of the samples indicating that the nanoclay induced plastic deformation in solid PLA–12%(H2004 + PA). On the other hand, the addition of (H20 + PA) did not lead to higher ductility in the solid PLA.

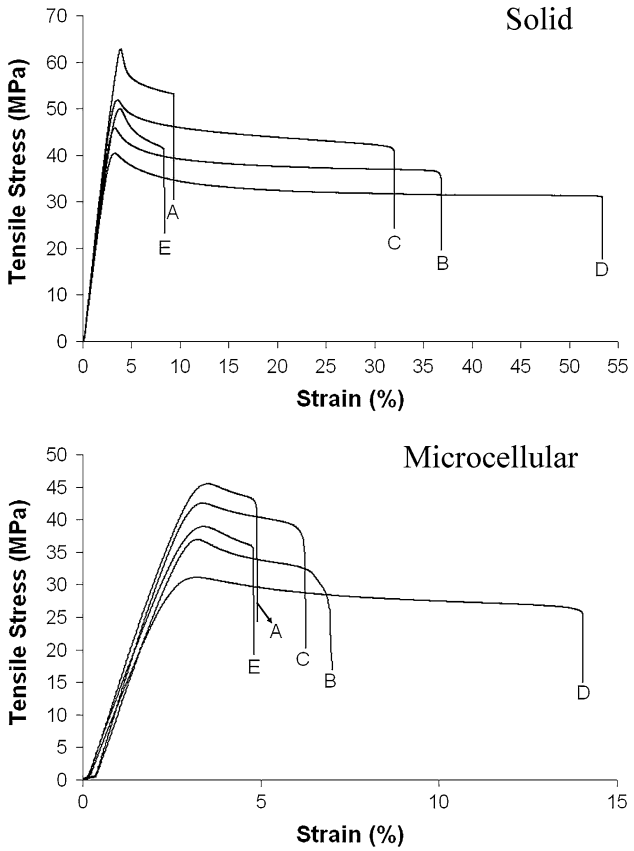

Fig. 9 Tensile stress–strain curves of solid and microcellular PLA and PLA–HBP blends: (*a*) pure PLA, (*b*) PLA–6%(H2004 + PA), (*c*) PLA–12%(H2004 + PA), (*d*) PLA–12%(H2004 + PA)–2% Nanoclay, (*e*) PLA–12%(H20 + PA)

The microcellular specimens showed a similar trend as that of the solid samples, but the solid samples had a much higher ductility than the microcellular specimens. This can be attributed to the presence of certain large cells that decreased the effective load bearing area and/or served as stress concentrators in the microcellular samples [54]. Overall, among all solid and microcellular specimens, PLA–12%(H2004 + PA)–2%Nanoclay composite showed the highest ductility.

The specific tensile properties of PLA and PLA–HBP blends are shown in Fig. 10. The left set of plots show the effect of (H2004 + PA) content and nanoclay; the right set of plots shows the effect of addition of different HBPs (H20 and H2004) on various mechanical properties of the material systems. Figure 10a shows the specific toughness of PLA and PLA–HBP blends. Fracture toughness, which is the energy-to-fracture per unit volume of the specimen, is obtained by integrating the area under the stress–strain curve [85]. Among the solid specimens, addition of 6%(H2004 + PA) increased the toughness of solid PLA by ~240% (Fig. 10a). However, by increasing the content of (H2004 + PA) to 12%, the toughness increased to 275%. This is a significant achievement in terms of toughness increase. Further, owing to addition of 2% nanoclay to the solid PLA–12%(H2004 + PA)–2%Nanoclay composite, the toughness increased to a gigantic value of 405%. This finding agrees with those from previous studies which showed that addition of two nanoscale fillers simultaneously can result in significantly enhanced properties [86]. Conversely, addition of 12% (H20 + PA) decreased the toughness by about 16% compared with solid PLA. This might be due to the higher cross-linking density induced between H20 and PA because it has more –OH groups (16) on the periphery compared with H2004 (6). A similar trend was observed for the microcellular specimens. Addition of 6%(H2004 + PA) resulted in ~97% increase in the toughness of microcellular PLA. Increasing the (H2004 + PA) content to 12%, the toughness increased to 191%. Moreover, owing to the addition of 2% nanoclay, the toughness of PLA–12%(H2004 + PA)–2%Nanoclay composite increased to about 334%. The decrease in the toughness of microcellular PLA–12%(H20 + PA) sample

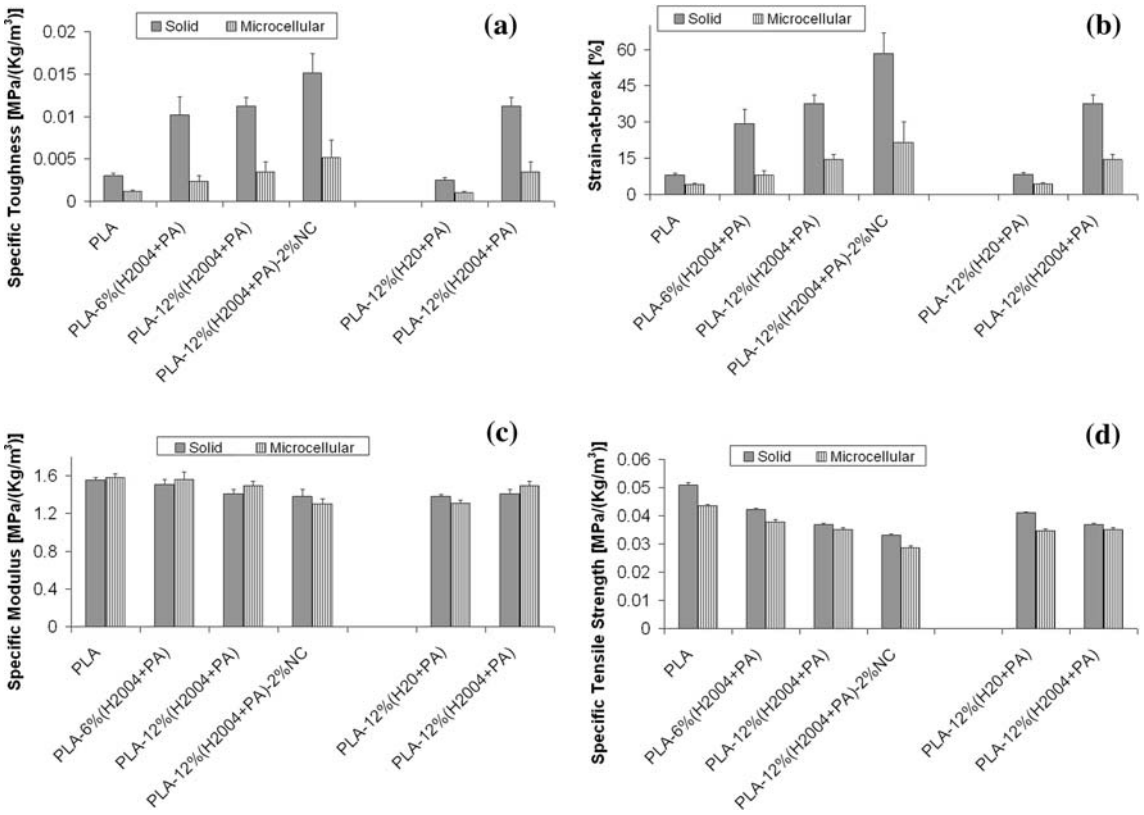

Fig. 10 Tensile properties of solid and microcellular PLA and PLA–HBP blends: **a** specific toughness, **b** strain-at-break, **c** specific modulus, **d** specific tensile strength

compared with microcellular PLA was 15%. Finally, compared with the solid samples, the toughness of microcellular samples was lower, possibly due to certain large voids in the microcellular specimens due to the dynamic nature of microcellular injection molding [54].

As with toughness, the strain-at-break of PLA (for both solid and microcellular) increased for PLA–6%(H2004 + PA), PLA–12%(H2004 + PA), and PLA–6%(H2004 + PA)–2%Nanoclay composite but decreased for PLA–12%(H20 + PA) (Fig. 10b). Also the strain-at-break values of the microcellular specimens were lower than those of their solid counterparts.

The specific tensile modulus is shown in Fig. 10c. Addition of HBP + PA slightly decreased the specific modulus. Among the solid specimens, addition of 6% and 12%(H2004 + PA) decreased the specific modulus of solid PLA by 3% and 10%, respectively. However, addition of 2% nanoclay did not have any effect on the specific modulus of solid PLA–12%(H2004 + PA). This may be due to the fact that the nanoclays were not fully exfoliated in the PLA matrix, as is evident from the TEM images (Fig. 2) and XRD data (Fig. 1). Addition of 12%(H20 + PA) reduced the specific modulus by 11%. Thus, PLA–12%(H20 + PA) and PLA–12%(H2004 + PA) had a similar effect on the specific moduli of the specimens. In general, the specific moduli of the microcellular specimens showed a similar trend that of solid. However, the reduction in specific moduli of the microcellular PLA–HBP blends was less compared with that of the solid samples. For example, addition of 6%(H2004 + PA) did not significantly reduce the specific modulus of the microcellular PLA, and addition of 12%(H2004 + PA) reduced the specific modulus by only 5%.

Figure 10d shows the specific tensile strength of all the solid and microcellular specimens. The specific strength of all samples was less than that of pure PLA (solid or microcellular). Various strategies used to toughen a material often results in a dramatic reduction in strength [39]. In this study, the reduction in strength was observed to be 17–35% for solid and 13–34% for microcellular specimens. In microcellular specimens, lower strength reductions were found when HBP was added to PLA compared to the solid specimens. Compared with solid samples, microcellular samples had lower average specific strengths. Again, this might be caused by certain large voids in the microcellular specimens due to the dynamic nature of the microcellular injection-molding process [54]. Such large voids may concentrate stress, thereby decreasing mechanical properties.

Conclusions

Solid and microcellular polylactide (PLA) and HBP blends were injection-molded using conventional and microcellular processes. For microcellular samples, a weight reduction of 10–16% was achieved. The solid and microcellular PLA–12%(H2004 + PA)–2%Nanoclay composites revealed an intercalated structure based on the XRD and TEM analyses. A quantitative analysis of the cell morphology of the microcellular specimens showed that the addition of HBPs and nanoclay decreased the average cell size, and increased the cell density.

For all the solid and microcellular specimens, the degree of crystallinity increased with the addition of HBPs + PA and nanoclay. Also, no significant difference was observed between the degree of crystallinity of the corresponding solid and microcellular samples. The storage moduli of both the solid and microcellular samples decreased compared with pure PLA. Among all the solid and microcellular PLA–HBP blends, PLA–12%(H2004 + PA)–2%Nanoclay composites exhibited the highest specific toughness (e.g., 405% increase for the solid specimen and 334% increase for the microcellular specimen) and strain-at-break (e.g., 626% increase for the solid specimen and 406% increase for the microcellular specimen) followed by PLA–12%(H2004 + PA) and PLA–6%(H2004 + PA). On the other hand, PLA–12%(H20 + PA) had a similar specific toughness and strain-at-break values as the pure PLA for both solid and microcellular samples. Furthermore, the addition of HBPs + PA and HBP–nanoclay caused a slight reduction in specific modulus and a considerable reduction in specific strength compared with pure PLA in all solid and microcellular PLA–HBP blends. Finally, the microcellular samples exhibited lower specific toughness, strain-at-break, and specific strength compared with their solid counterparts.

Acknowledgements We would like to acknowledge the financial support from National Science Foundation (CMMI-0544729), the USDA Forest Products Laboratory for the use of its equipment to compound the materials and Perstorp Polyols Inc., USA for donating the Boltorn HBPs.

References

1. Carole TM, Pellegrino J, Paster MD (2004) Appl Biochem Biotechnol 113–116:871
2. Gross RA, Kalra B (2002) Science 297(5582):803
3. Kuriam JV (2005) In: Mohanty AK, Misra M, Drzal LT (eds) Natural fibers, biopolymers, and biocomposites. CRC press, Boca Raton
4. Mohanty AK, Misra M, Drzal LT (2002) J Polym Environ 10(1–2):19
5. Pilla S, Gong S, O'Neill E, Yang L, Rowell RM (2009) J Appl Polym Sci 111(1):37
6. Bhardwaj R, Mohanty AK (2007) J Biobased Mater Bioenergy 1:191
7. Heino A, Naukkarinen A, Kulju T, Törmälä P, Pohjonen T, Mäkelä EA (1996) J Biomed Mater Res 30:187
8. Luciano RM, Zavaglia CAC, Duek EAR, Alberto-Rincon MC (2003) J Mater Sci Mater Med 14:87
9. Itoh E, Matsuda S, Yamauchi K, Oka T, Iwata H, Yamaoka Y, Ikada Y (2000) J Biomed Mater Res 53:640
10. Bleach NC, Nazhat SN, Tanner KE, Kellomaki M, Tormala P (2002) Biomaterials 23:1579
11. Furukawa T, Matsusue Y, Yasunaga T, Shikinami Y, Okuno M, Nakamura T (2000) Biomaterials 21:889
12. Park YJ, Nam KH, Ha SJ, Pai CM, Chung CP, Lee SJ (1997) J Controlled Release 43:151
13. Giardino R, Fini M, Aldini NN, Giavaresi G, Rocca M (1999) J Trauma 47:303
14. Lee SH, Kim BS, Kim SH, Kang SW, Kim YH (2004) Macromol Biosci 4:802
15. Pego AP, Siebum B, Van Luyn MJA, Gallego Y Van Seijen XJ, Poot AA, Grijpma DW, Feijen J (2003) Tissue Eng 9:981
16. Auras R, Harte B, Selke S (2004) Macromol Biosci 4:835
17. Grijpma DW, Zondervan GJ, Pennings AJ (1991) Polym Bull 25:327
18. Wehrenberg RH (1981) Mater Eng 94:63
19. Hiljanen-Vainio M, Karjalainen T, Seppala JV (1996) J Appl Polym Sci 59:1281
20. Hiljanen-Vainio M, Orava PA, Seppala JV (1997) J Biomed Mater Res 34:39
21. Buchholz B (1993) J Mater Sci Mater Med 4:381
22. Nakayama A, Kawasaki N, Arvanitoyannis I, Iyoda J, Yamamoto N (1995) Polymer 36(6):1295
23. Joziasse CAP, Grablowitz H, Pennings AJ (2000) Macromol Chem Phys 201:107
24. Kylma J, Seppaela JV (1997) Macromolecules 30(10):2876
25. Storey RF, Wiggins JS, Puckett AD (1994) J Polym Sci Part A 32(12):2345
26. Stolt M, Hiltunen K, Sodergard A (2001) Biomacromolecules 2(4):1243
27. Aslan S, Calandrelli L, Laurienzo P, Malinconico M, Migliaresi C (2000) J Mater Sci Mater Med 35(7):1615
28. Hiljanen-Vainio M, Varpomaa P, Seppala J, Tormala P (1996) Macromol Chem Phys 197(4):1503
29. Maglio G, Migliozzi A, Palumbo R, Immirzi B, Volpe MG (1999) Macromol Rapid Commun 20(4):236
30. Maglio G, Malinconico M, Migliozzi A, Groeninckx G (2004) Macromol Chem Phys 205(7):946
31. Meredith JC, Amis E (2000) Macromol Chem Phys 201(6):733
32. Kylma J, Hiljanen-Vainio M, Seppala J (2000) J Appl Polym Sci 76(7):1074
33. Kylma J, Seppala J (2000) J Appl Polym Sci 79(8):1531
34. Shibata M, Inoue Y, Miyoshi Y (2006) Polymer 47:3557
35. Hiljanen-Vainio M, Kylmae J, Hiltunen K, Seppaelae JV (1997) J Appl Polym Sci 63(10):1335
36. Ljungberg N, Wesslen B (2005) Biomacromolecules 6:1789
37. Martin O, Averous L (2001) Polymer 42:6209
38. Bhardwaj R, Mohanty AK (2007) Biomacromolecules 8:2476
39. Lin Y, Zhang KY, Dong ZM, Dong LS, Li YS (2007) Macromolecules 40:6257
40. Wong S, Shanks RA, Hodzic A (2004) Macromol Mater Eng 289:447
41. Zhang W, Zhang Y, Chen Y (2008) Iran Polym J 17(12):891
42. Zhang JF, Sun X (2004) Polym Int 53:716
43. Jiang L, Wolcott MP, Zhang J (2006) Biomacromolecules 7:199
44. Seiler M (2002) Chem Eng Technol 25(3):237
45. Hong Y, Coombs SJ, Cooper-White JJ, Mackay ME, Hawker CJ, Malmstrom E, Rehnberg N (2000) Polymer 41:7705

46. Jannerfeldt G, Boogh L, Manson JAE (2000) Polymer 41:7627
47. Kil SB, Augros Y, Leterrier Y, Manson JAE (2003) Polym Eng Sci 43(2):329
48. Mezzenga R, Boogh L, Manson JAE (2001) Compos Sci Technol 61(5):787
49. Okonishnikov GB, Blednykh EI, Skripov Mekh VP (1973) Polimerov 2:370
50. Martini JE, Waldman FA, Suh NP (1982) In: SPE ANTEC Technical Papers, 28: 674
51. Naguib HE, Park CB, Reichelt N (2004) J Appl Polym Sci 91:2661
52. Pilla S, Kramschuster A, Gong S, Chandra A, Turng LS (2007) Int Polym Proc XXII(5):418–428
53. Kramschuster A, Pilla S, Gong S, Chandra A, Turng LS (2007) Int Polym Proc XXII(5):436–445
54. Kramschuster A, Gong S, Turng LS, Li T, Li T (2007) J Biobased Mater Bioenergy 1:37
55. Kramschuster A, Cavitt R, Ermer D, Chen Z, Turng LS (2005) Polym Eng Sci 45(10):1408
56. Naguib HE, Park CB, Lee PC (2003) J Cell Plast 39(6):499
57. Pilla S, Kramschuster A, Lee J, Auer GK, Gong S, Turng LS (2009) Compos Interfaces 16(7–9):869
58. Chandra A, Gong S, Yuan M, Turng LS (2005) Polym Eng Sci 45(1):52
59. Yuan M, Winardi A, Gong S, Turng LS (2005) Polym Eng Sci 45:773
60. Gong A, Turng L-S, Park CB, Liao L (2008) In: Mohanty AK, Misra M, Nalwa HS (eds) Packaging nanotechnology. American Scientific Publishers, USA
61. Kwag C, Manke CW, Gulari E (1999) J Polym Sci B 37(19):2771
62. Royer JR, Gay YJ, Desimone JM, Khan SA (2000) J Polym Sci B 38(23):3168
63. Kwag C, Manke CW, Gulari E (2001) Ind Eng Chem Res 40(14):3048
64. Suh NP (1996) In: Stevenson JF (ed) Innovation in polymer processing-molding. Hanser Publishers, Munich
65. Gong S, Yuan M, Chandra A, Winardi A, Osorio A, Turng L-S (2005) Int Polym Proc 2:202
66. Throne J (1979) In: Suh NP, Sung N (eds) Science and technology of polymer processing. MIT Press, Cambridge, MA, USA
67. Singh S, Ray SS (2007) J Nanosci Nanotechnol 7:2596
68. Pilla S, Gong S, Turng LS (2010) In: Mittal V (ed) Polymer nanotube nanocomposites. Wiley-Scrivener, MA, USA
69. Rezgui F, Swistek M, Hiver JM, G'Sell C, Sadoun T (2005) Polymer 46(18):7370
70. Garlotta D (2002) J Polym Environ 9:63
71. Nam JY, Ray SS, Okamoto M (2003) Macromolecules 36(19):7126
72. Wang H, Sun XZ, Seib P (2003) J Appl Polym Sci 90:3683
73. Naguib HE, Park CB, Reichelt N, Panzer U (2002) Polym Eng Sci 42(7):1481
74. Lee LJ, Zheng C, Cao X, Han X, Shen J, Xu G (2005) Compos Sci Technol 65(15–16):2344
75. Kharbas H, Nelson P, Yuan M, Gong S, Turng LS (2003) Polym Compos 24(6):655
76. Hodge IM (1983) Macromolecules 16(6):898
77. Hodge IM, Huvard GS (1983) Macromolecules 16(3):371
78. Behrens AR, Hodge IM (1982) Macromolecules 15(3):756
79. Turi EA (1997) Thermal characterization of polymeric materials. Academic Press, USA
80. Masirek R, Kulinski Z, Chionna D, Piorkowska E, Pracella M (2007) J Appl Polym Sci 105(1):255
81. Pracella M, Chionna D, Anguillesi I, Kulinski Z, Piorkowska E (2006) Compos Sci Technol 66(13):2218
82. Yasuniwa M, Tsubakihara S, Sugimoto Y, Nakafuku C (2004) J Polym Sci B 42:25
83. Wang Y, Funari SS, Mano JF (2006) Macromol Chem Phys 207:1262
84. Pothan LA, Thomas S, Groeninckx G (2006) Compos A 37(9): 1260
85. Van Vlack LH (1989) Elements of materials science and engineering. Addison-Wesley Publishing Company, USA
86. Yang L, Zhang C, Pilla S, Gong S (2008) Compos A 39:1653